Title
Energy decomposition analysis for exciplexes using absolutely localized molecular orbitals

Journal
The Journal of Chemical Physics, 148(6)

ISSN
0021-9606

Authors
Ge, Qinghui
Mao, Yuezhi
Head-Gordon, Martin

Publication Date
2018-02-14

DOI
10.1063/1.5017510

Peer reviewed

Energy decomposition analysis for exciplexes using absolutely localized molecular orbitals

Qinghui Ge, Yuezhi Mao, and Martin Head-Gordon

Citation: The Journal of Chemical Physics **148**, 064105 (2018); doi: 10.1063/1.5017510
View online: https://doi.org/10.1063/1.5017510
View Table of Contents: http://aip.scitation.org/toc/jcp/148/6
Published by the American Institute of Physics

Energy decomposition analysis for exciplexes using absolutely localized molecular orbitals

Qinghui Ge,[1,2] Yuezhi Mao,[1] and Martin Head-Gordon[1,2,a)]
[1]*Kenneth S. Pitzer Center for Theoretical Chemistry, Department of Chemistry, University of California at Berkeley, Berkeley, California 94720, USA*
[2]*Chemical Science Division, Lawrence Berkeley National Laboratory, Berkeley, California 94720, USA*

(Received 27 November 2017; accepted 21 January 2018; published online 9 February 2018)

An energy decomposition analysis (EDA) scheme is developed for understanding the intermolecular interaction involving molecules in their excited states. The EDA utilizes absolutely localized molecular orbitals to define intermediate states and is compatible with excited state methods based on linear response theory such as configuration interaction singles and time-dependent density functional theory. The shift in excitation energy when an excited molecule interacts with the environment is decomposed into frozen, polarization, and charge transfer contributions, and the frozen term can be further separated into Pauli repulsion and electrostatics. These terms can be added to their counterparts obtained from the ground state EDA to form a decomposition of the total interaction energy. The EDA scheme is applied to study a variety of systems, including some model systems to demonstrate the correct behavior of all the proposed energy components as well as more realistic systems such as hydrogen-bonding complexes (e.g., formamide-water, pyridine/pyrimidine-water) and halide (F^-, Cl^-)-water clusters that involve charge-transfer-to-solvent excitations. *Published by AIP Publishing.* https://doi.org/10.1063/1.5017510

I. INTRODUCTION

Environmental effects on ground states are the basis of solvation phenomena which are well-known to strongly affect solute molecular properties and chemical reactivity. Since electronically excited states involve less strongly bound electrons, often with much larger polarizabilities, environmental effects on such states will typically be larger as well as less chemically intuitive than for ground states. One example is the study of the solvent effects on excitation energies, i.e., solvatochromism. Most dielectric continuum models[1–3] and combined quantum mechanics and molecular mechanics (QM/MM) methods[4–6] focus on the electrostatic effect (permanent and induced) of solvent on the solute molecules. Other studies also pointed out that intermolecular Pauli repulsion is important especially when the solute excited states are rather diffuse,[7] and recently Kongsted and co-workers addressed this problem by introducing an effective confinement of the solute wavefunction.[8,9] Another interesting topic is the charge-transfer-to-solvent (CTTS) spectra,[10] a unique class of electronic spectra which are present in dipolar (e.g., aqueous) solution of small inorganic anions such as halides, OH^-, and NO_3^-. These anions undergo ionization rather than excitation in their gas phase but can form stable excited states in solutions. There have been extensive experimental[11–13] and theoretical[14–19] studies on the CTTS spectra, and this phenomenon is often explained by transfer of charges from anions to solution, where the delocalized electron is stabilized by the surrounding solvent molecules.

Electrostatics, dispersion, and polarization (POL) are the three types of long-range forces by which non-overlapping molecules interact.[20] In addition, Pauli repulsion and charge transfer (CT) are well-known repulsive and attractive forces between overlapping molecules. However, the definition of all terms in the overlapping regime is inherently non-unique. Energy decomposition analysis (EDA) decomposes the total interaction energy into several scalars corresponding to the aforementioned terms, thereby allowing an assessment of their relative importance. Many EDA schemes have been proposed and used for studying intermolecular interactions between molecules in their ground states, as discussed below. However, there are very few reported EDA approaches for excited states. Recently, Slipchenko *et al.* reported the hybrid QM/EFP (effective fragment potential) model[21–23] for studying excited states in the presence of a solvent environment. Other approaches aiming to construct the effective potential exerted by the environment as a combination of several physically meaningful components, such as the frozen density embedding (FDE)[24–26] and polarizable density embedding (PDE)[8,9,27] schemes, can also be utilized to model solvatochromic shifts. The fragment molecular orbital (FMO) method has also been extended to excited states[28] and used to distinguish the role of POL and CT on examples of solvatochromism. Excited states of large clusters can also be treated by *ab initio* implementations of the Frenkel-Davydov exciton model,[29–31] which uses a basis of monomer excitations and reveals inter-monomer state mixings. These approaches all represent useful *adaptations* of numerical methods for

a)Electronic mail: mhg@cchem.berkeley.edu

interpretive purposes, rather than a systematic effort to *design* an excited state EDA.

Among the EDA schemes designed for ground state interactions, two main categories are symmetry-adapted perturbation theory (SAPT)[32–36] and variational approaches.[37–53] SAPT evaluates intermolecular interaction energies through a perturbative approach, and it also provides a decomposition of the resulting energies into electrostatic, exchange-repulsion, induction, and dispersion terms. Recent SAPT advances include efficiency improvements using Kohn-Sham density functional theory (KS-DFT)[54,55] and efforts to separate POL and CT in the induction term.[56–58] Variational EDA methods date back to the early Kitaura-Morokuma[37,38] [for the Hartree-Fock (HF) theory] and Ziegler-Rauk[39,40] (for the Xα method) approaches. Such methods partition intermolecular interaction energies by constructing constrained intermediate states whose energies are upper bounds to the true total energy.

The absolutely localized molecular orbital (ALMO)-EDA[51,52] [and the closely related block-localized wavefunction (BLW)-EDA[46–48,59]] is a more recent variational EDA that separates the total interaction into contributions from frozen (FRZ) interactions, POL, and CT. Its main feature is the use of two intermediate states: an antisymmetrized Heitler-London wavefunction constructed from converged MOs of the monomers directly (for the evaluation of FRZ) and a variationally optimized state whose associated AO-to-MO coefficient matrix is constrained to be fragment-block-diagonal (to separate POL and CT), using the so-called "self-consistent field for molecular interactions" (SCF-MI) approach.[60–62] Recent improvements to the ALMO-EDA include the development of the fragment electrical response function (FERF) model[63] that yields POL (and CT) energies with a meaningful complete basis set (CBS) limit, and a decomposition of the frozen term into contributions from permanent electrostatics, Pauli repulsion and dispersion.[64] These advances define the second generation of the ALMO-EDA method.[53] Additionally a new connection between ALMO-EDA energy contributions and experimental observables has been achieved with the "adiabatic" ALMO-EDA[65] that optimizes the structure and evaluates properties such as vibrational frequencies and dipole moments on each constrained potential energy surface.

Some recent developments encourage us to formulate an EDA scheme based on ALMOs for intermolecular interactions involving excited states. The first is the development of ALMO-CIS,[66] a local variant of the configuration interaction singles (CIS) method.[67,68] The ALMO-CIS wavefunction is constructed from superposition of on-fragment single excitations, i.e., from a fragment-localized occupied orbital, we only allow excitations to virtual orbitals that are tagged to the same fragment. ALMO-CIS excludes inter-fragment charge transfer in a natural way and one can prove that it conserves fragment Mulliken populations.[69] This suggests that the CT term can be defined as the difference between excited state energies evaluated by ALMO-CIS and standard CIS, generalizing the ground state CT which is the difference between converged SCF-MI and full SCF energies. The second development is that the ALMO-EDA has been recently extended from SCF wavefunctions to post-SCF methods at the MP2 level.[70,71] In MP2-ALMO-EDA, the MP2 correlation energy is separated into contributions from four components: FRZ, POL, CT, and dispersion, and the first three are then added to their counterparts in the Hartree-Fock ALMO-EDA. Here we may follow a similar procedure to formulate a CIS-based EDA, as the CIS wavefunction is generated from the HF wavefunction, and the CIS excited state energy can be expressed as a sum of the ground state (HF) energy and the excitation energy.

In this work, we present a new EDA scheme for the study of intermolecular interaction involving excited molecules based on CIS [or linear response theory for single excitations, to be more general, including time-dependent density functional theory (TDDFT),[67,72–74] particularly in the Tamm-Dancoff approximation (TDA)[75]]. We focus our methodology development on cases where the excitation can be assigned to a single molecule within a complex, as is appropriate for solvatochromism, for example. The remainder of the paper is organized as follows: In Sec. II, we outline the theory for this new ALMO-EDA scheme. We then present a series of case studies in Sec. III. Some limitations of the method are discussed in Sec. IV including types of systems where the current scheme could fail.

II. THEORY

The EDA presented here uses linear response theory for single substitutions to treat the excited state. In this section, we present the approach as generally as possible, using CIS in one or two specific places where it is necessary to illustrate the formalism. Thus the general expressions below may be specialized to the CIS case by identifying ground state energies as Hartree-Fock, $E = E_{\mathrm{HF}}$, unconstrained excited state energies as CIS, $E^* = E^*_{\mathrm{CIS}}$, and ALMO ground and excited states as ALMO-HF and ALMO-CIS, respectively. The EDA scheme is readily extensible to TDDFT in the TDA approximation (and we have implemented the method for this latter case also). Since nonorthogonal orbitals are used at the frozen and polarized levels, we occasionally need to employ tensor notation, where subscripts imply covariant quantities (like orbitals or matrix elements) and superscripts imply contravariant quantities such as excitation amplitudes.[76]

The interaction energy associated with an excited cluster is defined as the difference between the excited supersystem energy, E^*, and the corresponding sum of fragment energies, E^*_{frag}, with a counterpoise correction for basis set superposition error (BSSE),

$$\Delta E^{\bigstar}_{\mathrm{INT}} = E^* - E^*_{\mathrm{frag}} + \Delta E^*_{\mathrm{BSSE}}. \tag{1}$$

To define E^*_{frag}, we assume that one of the fragments (labeled as fragment 1) has an excitation energy lower than the other fragments, as might be the case for a solute embedded in a solvent cluster. In that way, E^*_{frag} is the sum of isolated fragment energies, with fragment 1 excited and the rest remaining in the ground state,

$$E^*_{\mathrm{frag}} = E^*_1 + \sum_{J>1} E_J. \tag{2}$$

Since $E^* = E + \omega$ and $E^*_{\text{frag}} = \sum_J E_J + \omega_1$ (ω_1 is the excitation energy of the isolated fragment $F1$), we can separate the contribution from ground state and excitation energy as

$$\Delta E^*_{\text{INT}} = \Delta E_{\text{INT}} + \Delta\omega_{\text{INT}}, \tag{3}$$

where $\Delta E_{\text{INT}} = E - \sum_J E_J$ is the ground state interaction energy and $\Delta\omega_{\text{INT}} = \omega - \omega_1$.

We note that there are different choices for the geometries of the isolated fragments as well as the complex. Using optimized ground state geometries for both fragments and complexes is appropriate for a vertical excitation as a model of absorption spectra. On the other hand, geometries optimized for excited states (E^* for the complex, E^*_1 for isolated fragment $F1$) are also required for studying emission spectra. We shall confine ourselves to the absorption case here.

First we briefly recapitulate the decomposition of the ground state interaction energy ΔE_{INT}. Given a fixed geometry of a complex, the first-generation ground state ALMO-EDA[51] decomposes the ground state interaction energy (ΔE) into frozen (FRZ), polarization (POL), and charge transfer (CT) contributions,

$$\Delta E_{\text{INT}} = \Delta E_{\text{FRZ}} + \Delta E_{\text{POL}} + \Delta E_{\text{CT}}. \tag{4}$$

The separation of these three terms is achieved by defining the frozen and polarized intermediate states. The frozen MO coefficient matrix is constructed by concatenating the isolated fragment MOs, and the energy of the frozen state (E_{FRZ}) is computed using the associated one-particle density matrix. At the polarized level, the MOs are relaxed subject to the constraint that the MO coefficient matrix is fragment-block-diagonal, i.e., the MOs are "absolutely localized."[51,60] The energy lowering relative to the frozen state defines the polarization energy (ΔE_{POL}). Finally, an unconstrained SCF calculation is performed for the whole system, yielding the fully relaxed ground state energy denoted as E. The ground state FRZ, POL, and CT terms are thus defined as

$$\Delta E_{\text{FRZ}} = E_{\text{FRZ}} - \sum_J E_J, \tag{5}$$

$$\Delta E_{\text{POL}} = E_{\text{POL}} - E_{\text{FRZ}}, \tag{6}$$

$$\Delta E_{\text{CT}} = E - E_{\text{POL}} + \Delta E_{\text{BSSE}}. \tag{7}$$

In the excited state EDA, we want to define the frozen and polarized wavefunctions for the excited system (and their associated energies E^*_{FRZ} and E^*_{POL}) so that the excited state interaction energy (ΔE^*_{INT}) can be decomposed into the same three terms as in the ground state EDA,

$$\Delta E^*_{\text{INT}} = \Delta E^*_{\text{FRZ}} + \Delta E^*_{\text{POL}} + \Delta E^*_{\text{CT}}. \tag{8}$$

For the reasons discussed in the Introduction, we use the ALMO-CIS wavefunction (or its TDDFT or TDDFT/TDA analog as appropriate) to describe the polarized excited system, whose energy is labeled as E^*_{POL}. The CT contribution to the excited state interaction energy is then accounted for by the difference between the unconstrained and polarized excited state energies (with basis set superposition error correction included also),

$$\Delta E^*_{\text{CT}} = E^* - E^*_{\text{POL}} + \Delta E^*_{\text{BSSE}}. \tag{9}$$

Recalling that in the ground state ALMO-EDA, $\Delta E_{\text{CT}} = E - E_{\text{POL}} + \Delta E_{\text{BSSE}}$, the CT term can also be rewritten as

$$\Delta E^*_{\text{CT}} = \Delta E_{\text{CT}} + \Delta\omega_{\text{CT}}, \tag{10}$$

where $\Delta\omega_{\text{CT}} = \omega - \omega_{\text{POL}} + \Delta E^*_{\text{BSSE}} - \Delta E_{\text{BSSE}}$.

Next, at the frozen level, we want to freeze both the orbitals and the excitation amplitudes. Then we calculate the frozen excitation energy using the isolated fragment amplitudes $\mathbf{t}_1$. The effect of other fragments on fragment 1's excitation energy enters only through the frozen Fock matrix. Specializing to CIS, we obtain

$$\omega_{\text{FRZ}} = \sum_{i,a,j,b\in F1} (F_{ab}S_{ij}t_1^{ia}t_1^{jb} - F_{ij}S_{ab}t_1^{ia}t_1^{jb}) + \sum_{i,a,j,b\in F1} \langle\psi_i\psi_b||\psi_a\psi_j\rangle t_1^{ia}t_1^{jb} + 2\sum_{i,a\in F1} F_{ia}z_1^{ia}, \tag{11}$$

The form of the first two terms in the above equation is the same as the non-orthogonal CIS energy with isolated fragment amplitudes, $\mathbf{t}_1$. The last term, which involves the occupied-virtual block of the relaxed density of the isolated fragment ($\mathbf{z}_1$), is a correction term that is necessary to obtain the correct electrostatics in the non-overlapping regime.[70] To understand this latter term, one should notice that at long distance, the frozen term is dominated by electrostatics and we expect

$$\frac{\partial\omega_{\text{FRZ}}}{\partial\mathbf{E}} = \boldsymbol{\mu}^1_{\text{CIS}}. \tag{12}$$

Differentiating the first two terms in Eq. (11) gives $\text{Tr}(\boldsymbol{\mu}\mathbf{P}_1)$, where $\boldsymbol{\mu}$ is the dipole matrix in the AO basis and $\mathbf{P}_1$ is the unrelaxed CIS difference density of fragment 1,

$$\begin{aligned} P_1^{ab} &= S_{ij}t_1^{ia}t_1^{jb}, \\ P_1^{ij} &= -S_{ab}t_1^{ia}t_1^{jb}. \end{aligned} \tag{13}$$

Only when the last term is present, the correct dipole moment, which is evaluated as $\text{Tr}(\boldsymbol{\mu}\tilde{\mathbf{P}}_1)$ using the relaxed density, $\tilde{\mathbf{P}}_1$, can be recovered. The same issue arose in the MP2-ALMO-EDA, where an additional term is also needed for the frozen energy (see Ref. 70 for further discussion). Even so, there remains some ambiguity in the overlapping regime, which we now resolve. When the fragments overlap, we force the virtual space to be orthogonal to the occupied space so as to make the excitation well defined. Moreover, we reorthogonalize the virtual orbitals within fragments so that in this projected-then-reorthogonalized basis, the fragment excited states remain properly orthogonal to each other.

The frozen and polarization interaction of the excited system is defined as

$$\Delta E^*_{\text{FRZ}} = \Delta E_{\text{FRZ}} + \omega_{\text{FRZ}} - \omega_1 = \Delta E_{\text{FRZ}} + \Delta\omega_{\text{FRZ}}, \tag{14}$$

$$\Delta E^*_{\text{POL}} = \Delta E_{\text{POL}} + \omega_{\text{POL}} - \omega_{\text{FRZ}} = \Delta E_{\text{POL}} + \Delta\omega_{\text{POL}}. \tag{15}$$

So far, we have defined the three terms in the EDA for excited states and shown that all these terms can be split into a contribution from the ground state (ΔE, obtained by the ground state ALMO-EDA) as well as corrections arising from the excitation energies ($\Delta\omega$). This is because with the linear response theory, the wavefunction at each level of EDA uses their ground state counterpart as a reference.

The decomposition of ΔE^* tells us the components of interaction between excited and unexcited fragments, while the decomposition of $\Delta\omega$ is useful to interpret phenomena such as solvatochromic shifts. There is no definite sign for the $\Delta\omega's$. For example, the sign of $\Delta\omega_{\mathrm{POL}}$ can depend on whether polarization in the excited state is more or less favorable than that in the ground state. Since ALMO-CIS and standard CIS use different molecular orbitals, the intra-fragment restriction on excitation amplitudes made in ALMO-CIS does not make the ALMO-CIS excitation energy an upper bound to full CIS, which means $\Delta\omega_{\mathrm{CT}}$ can sometimes be positive. Also, there is no guarantee for the relative magnitude of $\Delta\omega$ and ΔE, implying that in extreme cases $\Delta E^*_{\mathrm{POL}}$ and ΔE^*_{CT} can also be positive (which appears unintuitive). This possibility stems from the fact that the excited state is not treated in an equal manner as the ground state, as linear response theory is utilized to evaluate the excitation energies, which uses the ground state wavefunction as the reference.

The frozen interaction can be further decomposed. One simple scheme is to define the electrostatic term as the Coulomb interaction between charge distributions of isolated fragments (the "quasi-classical" definition of electrostatics),

$$\Delta E^*_{\mathrm{CLS\_ELEC}} = \sum_{I<J} \int\int \mathrm{d}\mathbf{r}_1 \mathrm{d}\mathbf{r}_2 \rho_I^{tot}(\mathbf{r}_1) r_{12}^{-1} \rho_J^{tot}(\mathbf{r}_2), \qquad (16)$$

where $\rho_I^{tot}(\mathbf{r}) = \rho_I^{ele}(\mathbf{r}) + \rho_I^{nuc}(\mathbf{r})$ is the sum of nuclear and electronic densities of an isolated fragment. We use the relaxed CIS state density for the excited fragment and HF density for the rest (or the appropriate DFT analogs).

The Pauli term is then defined as the remainder of the frozen energy,

$$\Delta E^*_{\mathrm{PAULI}} = \Delta E^*_{\mathrm{FRZ}} - \Delta E^*_{\mathrm{CLS\_ELEC}}. \qquad (17)$$

We note that the Pauli term defined in this way is contaminated by dispersion if TDDFT or TDA is used, especially when employing dispersion-corrected functionals. It has been shown that for the ground state, this could lead to a negative Pauli term in the long range, which is deemed unphysical. A more rigorous method has been proposed by Horn *et al.* to decompose the ground state interaction energy into electrostatic, Pauli, and dispersion terms.[64] This could potentially be generalized to excited states cases in the future.

III. APPLICATIONS' EXAMPLES

The excited state ALMO-EDA has been implemented in a development version of the Q-Chem electronic structure program.[77] As tests of our EDA scheme, we apply it to five diverse systems: (a) water-charge interaction, (b) neon-helium and helium dimers, (c) formamide-water dimer, (d) pyridine/pyrimidine-water, and (e) halide-water. For systems (a), (c), and (e), the geometries are optimized with MP2[78] and the 6-311++G(2d,2p) basis set,[79,80] and EDAs are performed at the CIS/aug-cc-pVTZ[81,82] level. For system (b), we also use MP2 for geometry optimization and CIS for EDA, but a modified 6-311(2+)G basis set is employed for the calculations for a better description of the Rydberg states. System (d) uses geometries provided by the supplementary material of a related study,[83] and the EDA is based on TDDFT with the Tamm-Dancoff approximation (TDA)[75] at the ωB97X-D[84]/6-311++G(d,p)[79] level of theory. Counterpoise corrections for BSSE are applied to all the EDA calculations.

A. Water-charge

The lowest singlet excited state of water is 1^1B_1, with primarily valence character.[85] We investigate its interaction with a +1 point charge placed on the bisector of the HOH angle (on the oxygen side, as shown in Fig. 1). This system is equivalent to H_3O^+, with one variable OH distance and two fixed distances. Since there is only one fragment involved, the ALMOs are the canonical MOs and ALMO-CIS is equivalent to full CIS. This means that the charge transfer term is zero by definition. To obtain the frozen and polarization terms, we need to compute (1) ω_1: the excitation energy of water in the absence of the point charge; (2) ω_{FRZ}: as defined in Eq. (11), where the amplitudes are frozen and the perturbation enters through the Fock matrix; (3) ω_{POL}: obtained from a full CIS calculation on water in the presence of the charge.

We scan the distance between water (using the center of nuclear charges) and the point charge to obtain potential energy curves for each level of excitation energies [Fig. 2(a)] and the distance dependence of $\Delta\omega_{\mathrm{FRZ}}$, $\Delta\omega_{\mathrm{POL}}$, and $\Delta\omega_{\mathrm{INT}}$ [Fig. 2(b)]. A necessary condition for our EDA scheme to be legitimate is that the frozen and polarization terms must have the correct long-range behavior. Since there is no Pauli repulsion in this case, we expect to see that the frozen term decays as R^{-2}, which is the correct behavior of a permanent charge-dipole interaction. The polarization term, on the other hand, should have an R^{-4} distance dependence, which is the character of a charge-induced dipole interaction. As shown in Fig. 2(c), for the data points beyond 10 Å, the plots of $\log(\Delta\omega_{\mathrm{FRZ}})$ and $\log(-\Delta\omega_{\mathrm{POL}})$ vs. $\log R$ have slopes −1.98 and −3.90, respectively, which are each quite close to the expected values.

In the short range, the repulsive frozen (electrostatic) term is simply a consequence of the sign-flipping of the water dipole upon excitation. The short-range behavior of the polarization term is more complicated as it is not monotonic. To understand the polarization behavior, we look at how water's ground and excited state dipole moments vary when a +1 point charge is approaching (Fig. 3). In the long range, the dipole moments of the ground and excited states have opposite

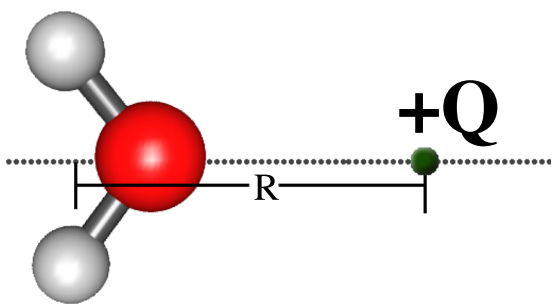

FIG. 1. Water molecule interacting with a point +1 charge. R is the distance between the center of nuclear charges of water and the point charge.

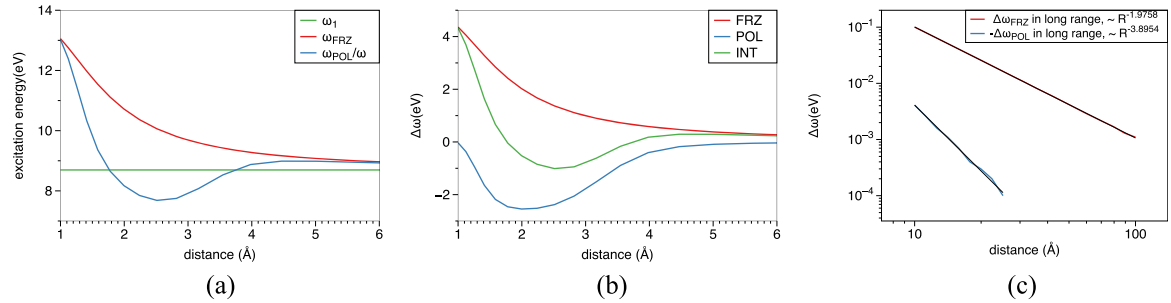

FIG. 2. (a) Excitation energy of water in the presence of a +1 charge at the isolated fragment (ω_1), frozen (ω_{FRZ}), and polarized (ω_{POL}) levels. (b) Decomposition of the shifts in excitation energy: the sum of the FRZ and POL contributions gives the total shift ("INT") due to the presence of +1 charge. (c) Plots of $\Delta\omega_{FRZ}$ and $\Delta\omega_{POL}$ vs. R at long range, on a logarithmic scale.

signs. Nonetheless, the positive charge always pulls electron density towards itself, and the induction effect is substantially stronger in the more polarizable excited state. Therefore, at short distances ($R < 4.5$ Å), the excited state dipole moment becomes even more negative than that of the ground state.

These facts are also reflected in the contour plots of electron densities (Fig. 4), from which we can see that at both 2.8 Å and 5.0 Å, the electrons move towards the charge and the changes in excited state densities are more substantial. The difference density $\Delta\rho = \rho^* - \rho$ has different patterns at 2.8 Å and 5.0 Å, which is consistent with the relative magnitude of dipole moments for ground and excited states. When the distance becomes smaller than 3 Å, the excited state dipole increases again. This is most likely because now the point charge penetrates the electron density of water and only part of its polarizing effect contributes to the decrease of the dipole moment. This does not happen to the ground state until R is close to 1 Å since the ground state electron density is less diffuse than that of the excited state.

B. Neon-helium dimer, clusters, and helium dimer

While the ground state binding energies of noble gas clusters are entirely due to dispersion interactions, which are neglected in CIS, shifts in the excitation energies of such clusters away from the atomic excitation can be well-described by CIS,[66,69,86] and our EDA can therefore be applied at that level. The first singlet excited state of Ne is a $2p \rightarrow 3s$ Rydberg state, at 18.4 eV, whereas the lowest singlet excited state of He ($1s \rightarrow 2s$) is much higher (21.1 eV). Therefore the lowest singlet excitation of the Ne–He dimer is expected to be Ne($2p \rightarrow 3s$) perturbed by the presence of helium. The Ne–He distance is scanned from 1 Å to 6 Å. The excitation energy is found to be blue-shifted for distances between 1.9 Å and 4.3 Å, which is mainly due to Pauli repulsion [see Fig. 5(b)]. As the Rydberg excited state is far more diffuse than the ground state, we expect greater Pauli repulsion at long distances for the excited state because of the increased overlap between the electronic density of helium and neon.

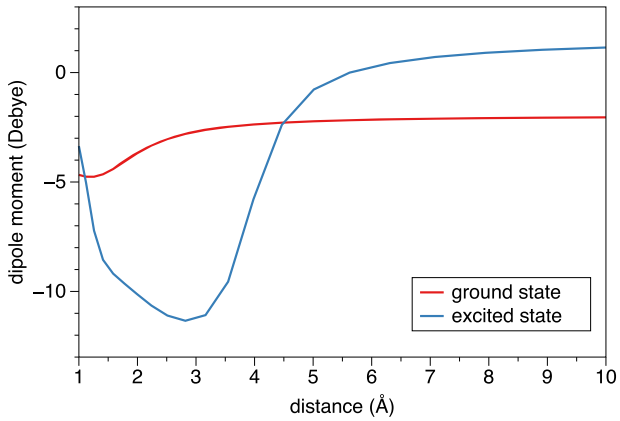

FIG. 3. Values of the ground and first excited state dipole moments of water varying with its distance from the +1 charge. When the point charge is absent, $\mu(\infty) = -1.98$ D, $\mu^*(\infty) = 1.51$ D.

From Fig. 5(b), it is interesting to see that the Pauli term begins to drop when the distance becomes smaller, and the excitation energy [Fig. 5(a)] exhibits a red shift for small enough distances. At small distances, the ground state is also subject to significant Pauli repulsion so that the difference between excited and ground states becomes less prominent. From Fig. 5(b), we also see that polarization is significantly more favorable for the excited state (i.e., the Rydberg excited state is far more polarizable than the ground state). CT is also slightly more favorable in the excited state for distances smaller than 4.4 Å.

The spectra of small helium clusters have been studied experimentally[87–89] and theoretically.[66,69,86] By examining the eigenstates, it has been shown that the red-edge states mainly come from surface excitations, while the blue-edge states have predominantly bulk character. To explore the origin of this effect with a model system, we perform an EDA on the excitation energies of $NeHe_N$ clusters, with one neon atom placed at the center and varying numbers of helium atoms around (see Fig. 6 for configurations). Every single atom is treated as an individual fragment in these calculations. As shown in Fig. 7, the blue shift of excitation energy comes from the Pauli repulsion term (the other terms are all negative). This is the main reason for a bulk state to be more blue-shifted than a surface state. In addition, the Pauli repulsion is roughly proportional to the number of helium atoms when N goes from 1 to 6. However, adding a second layer of 8 helium atoms ($N = 14$) barely charges the EDA result, as the interaction between the central neon and the second layer of helium atoms is very weak (the Pauli term decays exponentially with intermolecular distance).

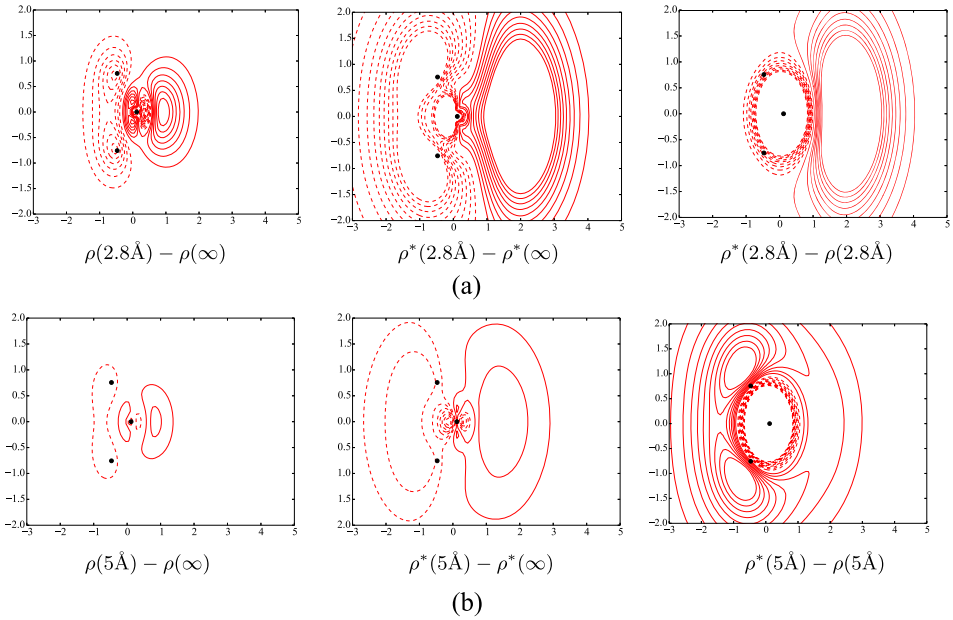

FIG. 4. Electron density difference (EDD) contours showing changes upon the excitation from the ground to first excited state of water in the presence of a +1 point charge located at R = (a) 2.8 Å and (b) 5 Å. In each row, the first and second panels exhibit the polarization effect due to the +1 point charge, and the third panel shows the difference between the ground and excited state densities. Values plotted are integrated to the molecular plane ($\Delta\rho(x, y) = \int dz \Delta\rho(x, y, z)$), and the contours are evenly spaced at $0.1e^-/\text{Å}^3$ with positive ones solid and negative ones dashed. The black dots indicate the positions of water's nuclei. (a) +Q at 2.8 Å, μ = −2.80 D, μ^* = −11.34 D. (b) +Q at 5.0 Å, μ = −2.23 D, μ^* = −0.19 D.

Finally, with some caution, we can also investigate the interaction between two helium atoms. As the two fragments are now identical, the excitation can reside on either helium when the fragments are isolated, so there are two degenerate reference states with excitation energy ω_0. We can use either as the reference, in the current EDA scheme, and they will yield degenerate frozen energies also. Note that one could break the degeneracy at the frozen level through the configuration interaction between these degenerate references (excitons). The effect of this "excitonic splitting" will be discussed in a future publication, but for now, it is included in the polarization term.

Keeping that in mind, we examine the potential energy curves for the helium dimer. The decomposition of excitation energies resembles the neon-helium system, but He–He has stronger polarization (more negative) and weaker Pauli repulsion (less positive) such that that the excitation energy is less blue-shifted at ∼3 Å and more red-shifted at small distances [Figs. 8(a) and 8(b)]. The interaction in the ground state is also less unfavorable for the helium dimer [Fig. 8(c)]. As a result of all these factors, the excited helium dimer is bound at small distances [Fig. 8(d)], while the interaction between an excited neon atom and a ground state helium atom is always unbound [Fig. 5(d)]. We also remind the reader that dispersion interactions are neglected in CIS theory: they would provide a small amount of additional binding in all states.

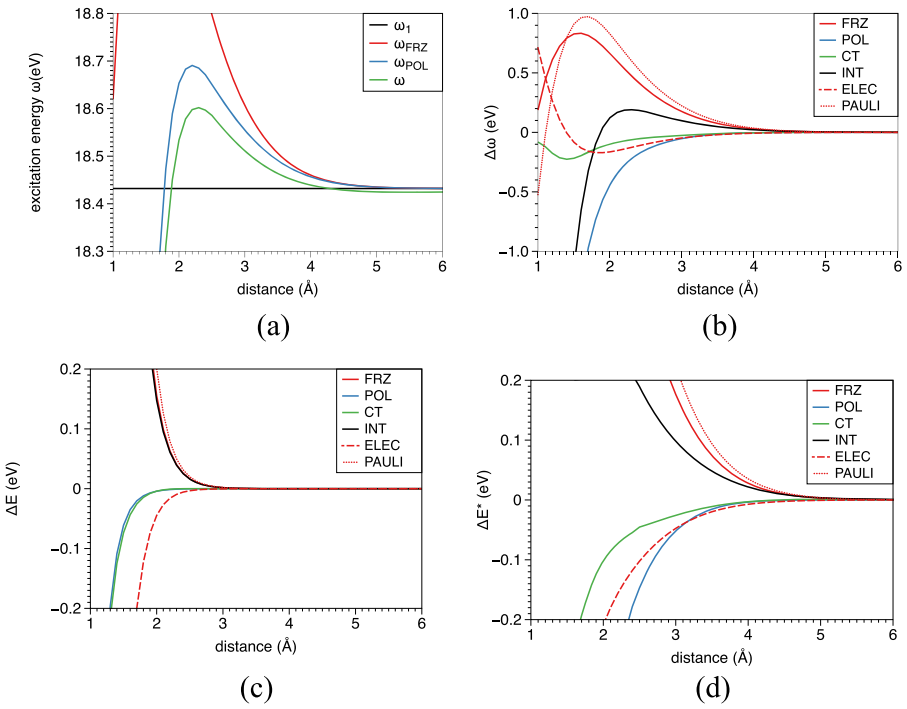

FIG. 5. EDA results for the Ne-He dimer (in eV): (a) excitation energies evaluated at different EDA levels; [(b)–(d)] decomposition of the shifts in excitation energies ($\Delta\omega$), ground state interaction energies (ΔE), and first excited state interaction energies (ΔE^*), respectively.

FIG. 6. Structures of the $NeHe_N$ clusters, where $N = 1, 2$ (linear), 4 (square), 6 (octahedron), 14 (face-centered cubic). The distances between the center neon and the first layer of helium atoms are 3.43 Å, which comes from a ground state geometry optimization of the Ne–He dimer at the MP2/6-311(2+)G level.

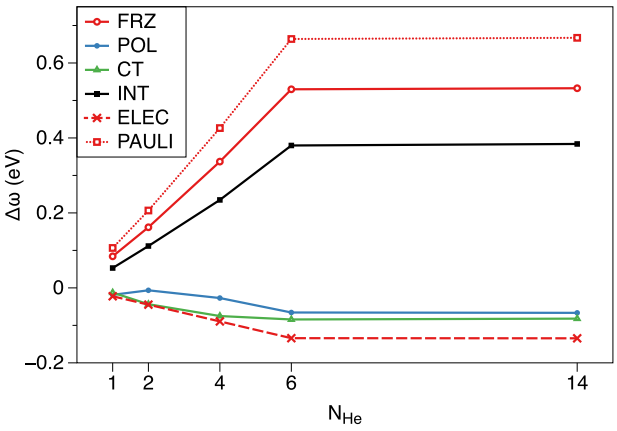

FIG. 7. Decomposition of the shifts in Ne's $2p \rightarrow 3s$ excitation energy (in eV) in $NeHe_N$ with varying numbers of helium atoms.

C. Formamide-water

Formamide is the simplest molecule that contains a peptide linkage. The first excited state of formamide is known as an $n \rightarrow \pi^*$ excitation.[90] Experimental studies have shown that in aqueous solutions, the $n \rightarrow \pi^*$ transition is blue-shifted by 0.27 eV compared to the gas phase result.[91,92] Gordon and co-workers performed a theoretical study using CIS on the formamide-water complexes with 1–3 water molecules and observed blue-shifted excitation energies in all calculations.[93]

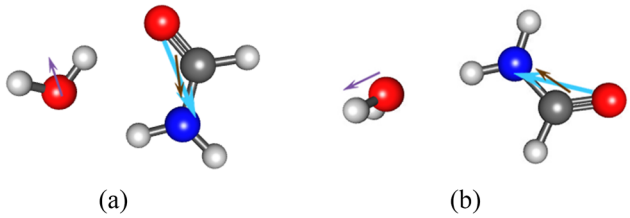

FIG. 9. Two configurations of the formamide-water complex. The geometries are optimized with MP2/6-311++G(2d,2p), as in Ref. 93. The ground and excited state dipole moments of formamide are indicated by blue and brown arrows, respectively, and the dipole moments of water are shown by purple arrows.

With one water molecule, they identified two possible configurations with different hydrogen-bond structures (shown in Fig. 9), where the (a) configuration is lower in energy and has a larger blue shift than (b).

Our EDA results in Table I indicate that the main reason for the blue shifts in both configurations is the frozen interaction, where electrostatics and Pauli repulsion both favor the ground state. It is reasonable that the excited state is subject to stronger Pauli repulsion, as the electronic density is typically more diffuse after excitation. The electrostatic interaction is less favorable in the excited state because when the lone pair electron is promoted to the empty π^* orbital, the carbonyl oxygen is not as negatively charged as in the ground state. To better understand the change in electrostatics, we first look at the dipole moments of water and formamide. In Fig. 9, we can see that the direction of formamide's dipole moment barely changes after excitation, while its magnitude is significantly reduced. This could result in a less favorable dipole-dipole interaction in the excited state for both configurations.

However, further investigation shows that only looking at the dipole-dipole interaction is probably not enough. In Table II, we report the electrostatic interaction energies calculated with a multipole expansion. When we pull the two

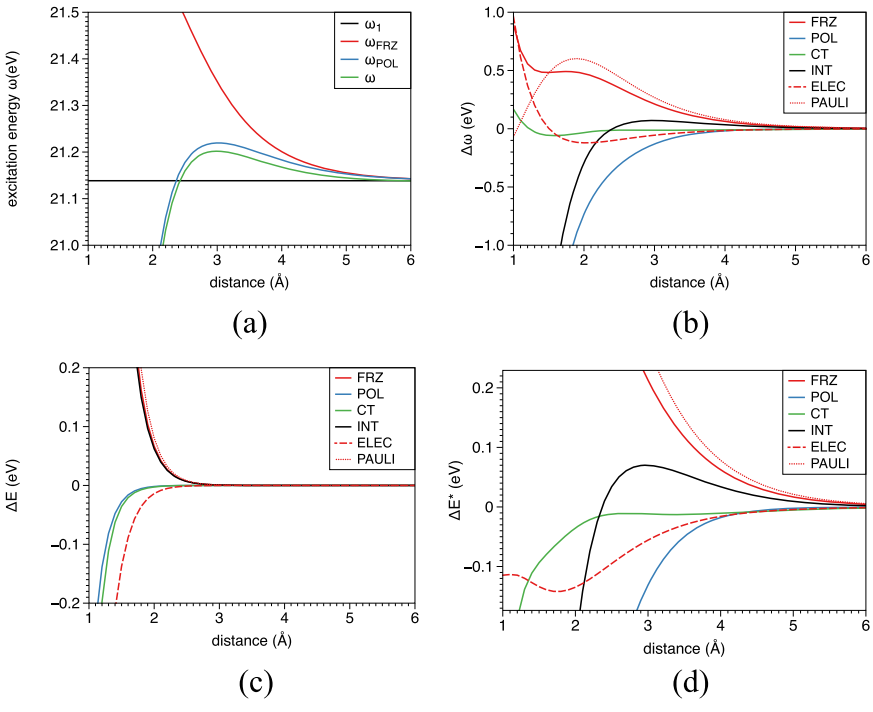

FIG. 8. EDA results for the helium dimer (in eV): (a) excitation energies evaluated at different EDA levels; [(b)–(d)] decomposition of the shifts in excitation energies ($\Delta\omega$), ground state interaction energies (ΔE), and first excited state interaction energies (ΔE^*), respectively.

TABLE I. EDA results for the formamide-water complex (in eV), including the decomposition of interaction energies in the ground state (ΔE) and the $n \rightarrow \pi^*$ excited state (ΔE^*) as well as the shifts in excitation energies ($\Delta\omega$).

	(a)					(b)				
	FRZ	(ELEC/PAULI)	POL	CT	INT	FRZ	(ELEC/PAULI)	POL	CT	INT
ΔE	−0.068	−0.758/0.691	−0.154	−0.085	−0.306	−0.087	−0.338/0.251	−0.056	−0.029	−0.172
ΔE^*	0.470	−0.353/0.823	−0.108	−0.318	0.045	−0.040	−0.297/0.257	−0.054	−0.036	−0.130
$\Delta\omega$	0.538	0.406/0.133	0.046	−0.233	0.351	0.047	0.041/0.006	0.002	−0.007	0.042

fragments apart, making the distance between the charge centers of water and formamide ∼10 Å, the Coulomb interaction evaluated by multipole expansion, truncated at the quadrupole-quadrupole level, recovers the classical electrostatics pretty well. However, at the equilibrium distance in (a) and (b), the multipole expansion energy is a very poor approximation to the classical electrostatic term. This fact suggests that at short distance, there is a non-negligible charge penetration effect due to the overlap of monomer densities, which makes the electrostatic interaction more favorable. Only at long distance can one safely employ the multipole interaction picture to interpret electrostatics.

Gordon *et al.* used the relative orbital energies of HOMO and LUMO to explain the origin of the blue shift.[93] Here, in Table III, we report the orbital energies of the dominant pair of natural transition orbitals (NTOs) (evaluated as $\langle\psi_{NTO}|\hat{F}|\psi_{NTO}\rangle$). The orbital energies of both occupied and virtual NTOs in configuration (a) are red-shifted from monomers to complexes, and the occupied one has a larger shift so the orbital energy difference is enlarged, which agrees with the picture discussed in Gordon's work. However, for the configuration (b), although we also observe the blue shifts in both occupied and virtual NTO energies, the orbital energy difference is red-shifted, which is opposed to the shift in the excitation energy. Moreover, the orbital energy difference of the NTO pairs is around 17 eV, which is much larger than the excitation energies (∼6.5 eV). On the other hand, we can consider looking at the excitation energy of a singly excited wavefunction Ψ_s where the transition takes place between the dominant NTO pair: $\omega_s = \langle\Psi_s|\hat{H}|\Psi_s\rangle - E_{HF}$. We find that ω_s recovers the CIS excitation energy ω quite well and has the correct blue-shifting behavior for both (a) and (b) configurations. This indicates that the excitation can be well described by a single orbital transition, but, in this case, the orbital energy difference is a poor approximation to the CIS excitation energy.

Finally, it is interesting to note that CT is more favorable for the excited state in configuration (a), i.e., $\Delta\omega_{CT} < 0$. This seems to be counterintuitive, as in (a), the $n \rightarrow \pi^*$ excitation renders the carbonyl oxygen less negatively charged, so one would expect weaker charge transfer than in the ground state. However, it may be problematic to relate the magnitude of CT energy lowering to the net charge flow between fragments. In some symmetric systems such as He_2, although there is no net charge transfer in both ground and excited states, CIS has lower excitation energy than ALMO-CIS, which is a result of allowing CT from the occupied orbitals of one fragment to the virtual orbitals of the other. From another perspective, the CT energy lowering in the ground state comes from removing the constraints on MOs (MOs no longer have

TABLE II. Comparison between the classical electrostatic terms given by our EDA scheme and results of multipole expansion (up to quadrupole moments) for the formamide-water system [with configurations (a) and (b) shown in Fig. 9]. "d" in subscripts represents dipoles and "q" is for quadrupoles. The energies are reported in eV.

	(a)				(b)			
	Distance (Å)	ΔE_{ELEC}	ΔE_{dd}	$\Delta E_{\text{dd+dq+qq}}$	Distance (Å)	ΔE_{ELEC}	ΔE_{dd}	$\Delta E_{\text{dd+dq+qq}}$
Ground state	2.7	−0.758	−0.240	−0.219	4.2	−0.338	−0.118	−0.154
	10.1	−0.005	−0.004	−0.005	10.2	−0.010	−0.009	−0.010
Excited state	2.8	−0.353	−0.098	0.002	4.0	−0.296	−0.067	−0.107
	10.3	−0.002	−0.002	−0.002	10.0	−0.006	−0.004	−0.005

TABLE III. NTO analysis for the formamide-water complex. The orbital energies of the dominant occupied-virtual NTO pair for the $n \rightarrow \pi^*$ excitation and the gap between them ($\Delta\epsilon$) are reported as well as the excitation energies estimated using the dominant natural transition (ω_s).

	(a)					(b)				
	$\epsilon_{\text{NTO}}^{(\text{occ})}$ (a.u.)	$\epsilon_{\text{NTO}}^{(\text{virt})}$ (a.u.)	$\Delta\epsilon$ (eV)	ω_s (eV)	ω (eV)	$\epsilon_{\text{NTO}}^{(\text{occ})}$ (a.u.)	$\epsilon_{\text{NTO}}^{(\text{virt})}$ (a.u.)	$\Delta\epsilon$ (eV)	ω_s (eV)	ω (eV)
Monomer	−0.437	0.187	16.992	6.537	6.448	−0.438	0.188	17.049	6.585	6.493
Complex	−0.450	0.180	17.131	6.899	6.799	−0.422	0.203	17.002	6.629	6.536

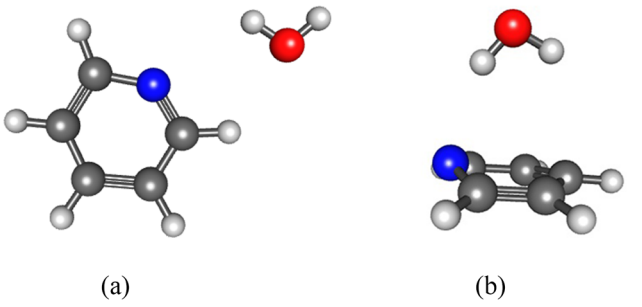

FIG. 10. The linear (a) and on-top (b) configurations for the pyridine-water complexes.

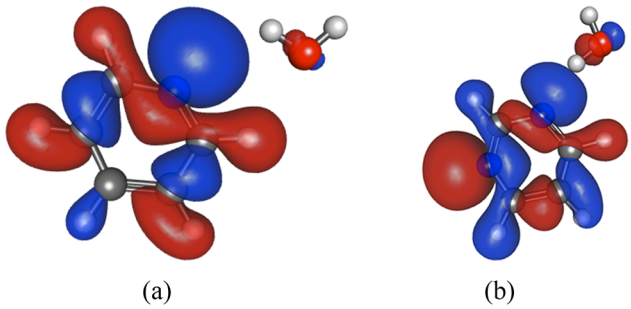

FIG. 11. The dominant occupied NTOs for the $n \rightarrow \pi^*$ excited states of the (a) pyridine- and (b) pyrimidine-water complexes in linear configuration.

to be block-diagonal), while in the excited state, both MOs and CIS amplitudes are relaxed (the amplitude corresponding to interfragment excitations can be non-zero). The additional variational degree of freedom in the CIS wavefunction is the main reason for CT usually causing a red shift in excitation energy.

D. Pyridine-water and pyrimidine-water

Hydrogen bonds between heteroaromatic rings, such as pyridine and diazines, and water are of great interest because of their roles in biological systems.[94–96] Typical geometric configurations include a linear hydrogen bond configuration and an "on-top" configuration where H_2O interacts with the π system (see Fig. 10 for illustration of these two configurations). A previous study[83] showed that the linear structure is more stable in the ground state of both pyridine and diazines. However, for the excited state, pyridine is more stable with the on-top structure, while the linear one is still preferred for pyridazine and pyrimidine. In order to gain more insight into this interesting fact, we perform EDA with the ωB97X-D functional on the pyridine-water and pyrimidine-water complexes, using the geometries given in the supplementary material of Ref. 83, which are optimized for the first excited state ($n \rightarrow \pi^*$) at the TDDFT ωB97X-D/6-311++G(d,p) level of theory. All data are collected in Table IV. The results of EDA with CIS, using the same geometries are also presented in Table S1 of the supplementary material) for comparison.

Our results show that upon excitation, the interaction between pyridine/pyrimidine and water becomes weaker in the linear structure but stronger in the top structure. Further decomposition shows that this is mainly an electrostatic effect. This is reasonable since we can imagine that during an $n \rightarrow \pi^*$ excitation, the electronic density of nitrogen's lone pair will move towards the π system, which weakens the hydrogen bond in the linear structure but strengthens the interaction between water and the heteroaromatic ring in the on-top configuration. For pyrimidine, the linear structure is

TABLE IV. EDA results for the pyridine- and pyrimidine-water complexes using the ωB97X-D functional. Presented data (in eV) include the decomposition of interaction energies in the ground state (ΔE) and the $n \rightarrow \pi^*$ excited state (ΔE^*) as well as the shifts in excitation energies ($\Delta\omega$). "gs" denotes that geometries optimized in the ground state are used.

Pyridine-water						
		FRZ	(ELEC/PAULI)	POL	CT	INT
Linear ($n \rightarrow \pi^*$)	ΔE	−0.140	−0.204/0.064	−0.024	−0.020	−0.184
	ΔE^*	−0.047	−0.126/0.079	−0.008	−0.047	−0.101
	$\Delta\omega$	0.093	0.078/0.015	0.017	−0.027	0.083
Top ($n \rightarrow \pi^*$)	ΔE	−0.077	−0.155/0.078	−0.032	−0.048	−0.157
	ΔE^*	−0.131	−0.249/0.117	−0.034	−0.054	−0.220
	$\Delta\omega$	−0.054	−0.094/0.039	−0.002	−0.007	−0.063
Linear (gs)	ΔE	−0.120	−0.519/0.399	−0.079	−0.120	−0.319
	ΔE^*	0.394	−0.105/0.499	−0.022	−0.408	−0.036
	$\Delta\omega$	0.514	0.414/0.100	0.057	−0.288	0.283
Pyrimidine-water						
		FRZ	(ELEC/PAULI)	POL	CT	INT
Linear ($n \rightarrow \pi^*$)	ΔE	−0.122	−0.530/0.408	−0.078	−0.119	−0.318
	ΔE^*	0.060	−0.399/0.459	−0.104	−0.216	−0.259
	$\Delta\omega$	0.182	0.131/0.052	−0.026	−0.097	0.059
Top ($n \rightarrow \pi^*$)	ΔE	−0.052	−0.210/0.159	−0.035	−0.059	−0.146
	ΔE^*	−0.072	−0.254/0.182	−0.038	−0.077	−0.187
	$\Delta\omega$	−0.020	−0.044/0.024	−0.003	−0.018	−0.041
Linear (gs)	ΔE	−0.128	−0.470/0.342	−0.066	−0.101	−0.296
	ΔE^*	0.164	−0.226/0.182	−0.095	−0.213	−0.144
	$\Delta\omega$	0.292	0.244/−0.160	−0.029	−0.112	0.152

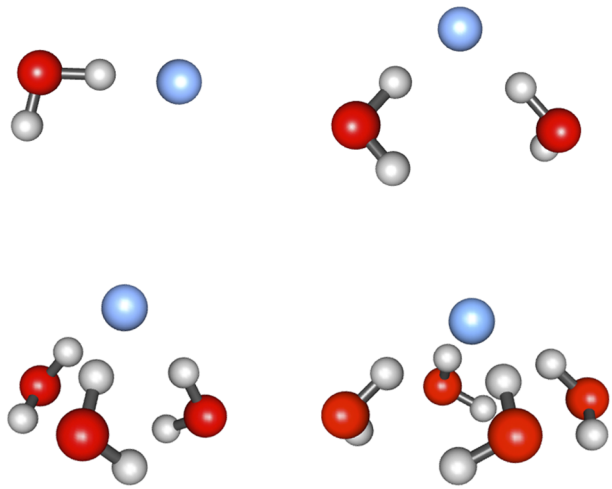

FIG. 12. Illustration of the structures for $X^-(H_2O)_N$ (N = 1, 2, 3, 4). N = 1 has the typical linear hydrogen bond geometry, while N = 2, 3, 4 have C_2-, C_3-, C_4-like symmetries.

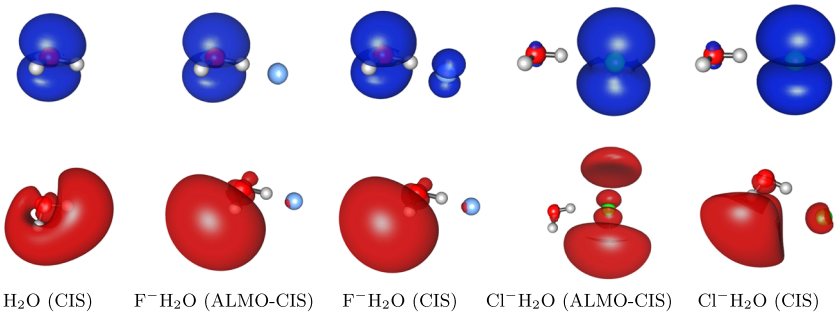

FIG. 13. Attachment (red) and detachment (blue) densities for the first excited states of an isolated water molecule and the $F^-(H_2O)$, $Cl^-(H_2O)$ complexes. For the latter two complexes, the results of both ALMO-CIS and standard CIS are plotted.

much more stable than the on-top one in the ground state (0.318 eV vs. 0.146 eV for the binding energy), so the above-mentioned effect does not reverse the order of stability for these two configurations in their excited states. However, in the excited state of pyridine, the on-top configuration becomes more favorable. All these are consistent with the findings in Ref. 83.

It is also interesting that for the linear structures, CT results in a much smaller energy lowering in pyridine than in pyrimidine, for both ground and excited states. A closer look at the optimal geometries of these exciplexes can help us understand why. For pyrimidine-water, the N–H–O angle is 161°, while for pyridine-water, this angle is much smaller (113°). An N–H–O angle that is far away from 180° indicates that the hydrogen bond is likely broken in pyridine-water's excited state. For pyrimidine, however, the non-bonding orbitals on both nitrogen atoms can contribute to the $n \rightarrow \pi^*$ transition, so the linearity of the hydrogen bond is less affected. The dominant occupied NTOs for the $n \rightarrow \pi^*$ excited states of both pyridine and pyrimidine (shown in Fig. 11) support this assumption, as the non-H-bonded nitrogen atom in pyrimidine is significantly involved in forming the occupied NTO. As a further investigation, we also perform EDAs on the linear structures optimized in the ground state. The resulting structures show typical hydrogen-bonding characters, as the N–H–O angles are 163° and 153° for pyridine and pyrimidine, respectively. With these structures, the energy lowering due to CT for these two complexes becomes more comparable, as shown in Table IV.

E. Halide-water

The final system is a challenging example for our current EDA scheme. Halide anions have bound excited states in solution but not in gas phase, which is due to the charge transfer to solvent (CTTS) effect that stabilizes the promoted electron. There have been various studies on the excited states of small halide-water clusters $X^-(H_2O)_N$, and the role of CTTS has been discussed.[14–19] Kim *et al.*[19] reported TDDFT and CIS excitation energies for X = F, Cl, Br, I, and N = 1–4. They observed a blue shift in excitation energies when N increases. By examining the amount of charge transfer upon excitation (measured as the change in Mulliken population on X^-), they also pointed out that the CTTS effect is minimal for F^- but significant for Cl^-, Br^-, and I^-.

We obtained geometries of $F^-(H_2O)_N$ and $Cl^-(H_2O)_N$ with N = 1–4, which are similar to the ones Kim *et al.* used in their studies (see Fig. 12). Starting from the simplest $N = 1$ case, we first look at the attachment density and detachment density at the ALMO-CIS and CIS levels (Fig. 13). For $F^-(H_2O)$, the excitation is mainly located on water. The main difference between ALMO-CIS and CIS is that the CIS detachment density has some small values on F^-. These are consistent with the conclusion in Ref. 19 that charge transfer in $F^-(H_2O)_N$ is small. For $Cl^-(H_2O)$, the detachment density looks similar in ALMO-CIS and CIS. However, when CT is allowed, the attachment density migrates from the vicinity of Cl^- to that of water. Based on the different character of excited states in $F^-(H_2O)_N$ and $Cl^-(H_2O)_N$, we made different choices for the fragment to excite at the isolated fragment level. For

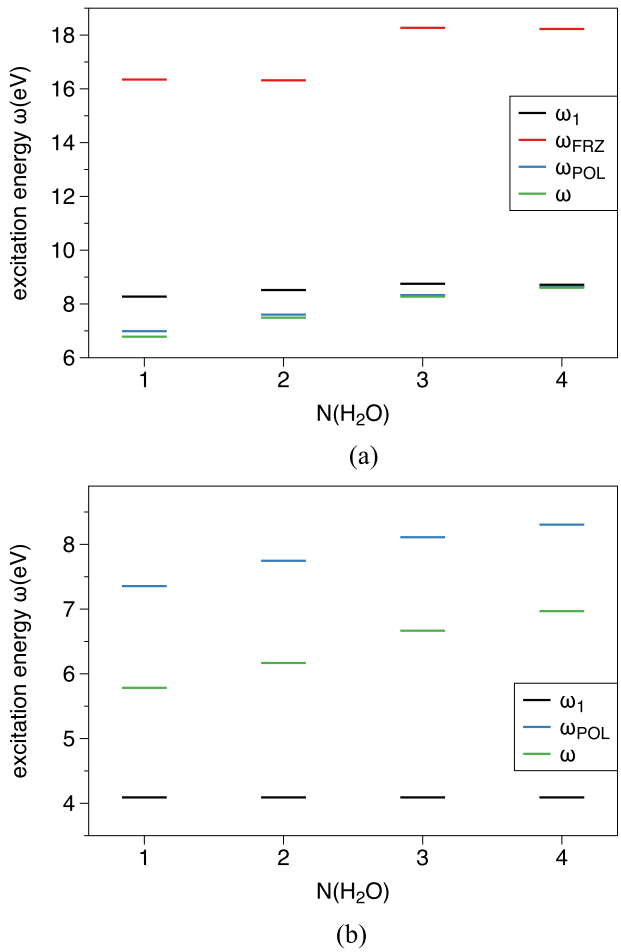

FIG. 14. Excitation energies (in eV) for $F^-(H2O)_N$ (a) and $Cl^-(H2O)_N$ (b) computed at different EDA levels. Note that ω_1 is given by the first excitation energy of the water molecules for the former system, while the HOMO energy of Cl^- is used for the latter system so that it does not vary with N.

TABLE V. EDA results (in eV) for the shifts in the lowest excitation energies ($\Delta\omega$) of the $F^-(H_2O)_N$ (a) and $Cl^-(H_2O)_N$ (b) systems.

	(a) $F^-(H_2O)_N$				
N	FRZ	(ELEC/PAULI)	POL	CT	INT
1	8.072	−0.803/8.875	−9.358	−0.203	−1.489
2	7.800	−0.746/8.545	−8.714	−0.112	−1.026
3	9.519	−0.745/10.264	−9.941	−0.052	−0.474
4	9.514	−0.709/10.223	−9.595	−0.027	−0.108

	(b) $Cl^-(H_2O)_N$		
N	NON-CT(FRZ+POL)	CT	INT
1	3.264	−1.572	1.693
2	3.656	−1.579	2.077
3	4.019	−1.444	2.575
4	4.214	−1.337	2.877

$F^-(H_2O)_N$, the water molecules are excited, which means ω_1 is the excitation energy of the water cluster evaluated in isolation (note that in our calculations for halide-water clusters, all the water molecules are treated as one single fragment). For $Cl^-(H_2O)_N$, the reference contains excited Cl^- and ground state water molecules. However, as Cl^- has no bound excited state, we take its ionization energy estimated by the HOMO energy of Cl^- as ω_1, which would be the "excitation energy" of a CIS calculation with the virtual one being a free electron. To avoid the complexity of redefining ω_{FRZ}, the electrostatics, Pauli repulsion, and polarization terms are combined into a single non-CT term by taking the difference between the ALMO-CIS excitation energy and ω_1.

Figure 14 shows the excitation energies at different EDA levels, and Table V summarizes the EDA results for the shifts in excitation energies. For $F^-(H_2O)_N$, it is surprising to see a Pauli repulsion as large as ∼10 eV. To understand this, we note that there is a significant difference between the attachment density of isolated water and that of $F^-(H_2O)$ (Fig. 13). It is clear that the excited electron would experience a strong Pauli repulsion from the electronic density around F^-, and the repulsion would be relieved when the system is allowed to polarize. In spite of this, we have reservations about the very large value of the Pauli terms. The effect of other terms decreases as N increases, indicating that the excitation is approaching the bulk limit of pure water. As for $Cl^-(H_2O)_N$, we do observe a relatively large contribution from CT, and its effect on the excitation energy becomes smaller for larger clusters. For both $F^-(H_2O)_N$ and $Cl^-(H_2O)_N$, the excitation energy is blue-shifted when the number of water molecules increases, which is primarily due to the growing magnitude of the unfavorable non-CT effect.

IV. CONCLUSION AND OUTLOOK

In the present paper, we have proposed an EDA scheme for intermolecular interactions that involve molecules in their excited states (i.e., exciplexes). In the spirit of the ground state ALMO-EDA, the energy partitioning is achieved by evaluating the excitation energy of the intermolecular complex at the frozen, polarized, and fully relaxed levels of linear response theory (using CIS as an example in the text below, but equally applicable to TDDFT). These intermediate states are defined by application of constraints to both the MOs and the CI coefficients (CIS amplitudes). The procedure is initiated with the evaluation of a target excited state on a specific isolated fragment. The frozen state is then constructed by embedding this electronically excited fragment into an environment described by ground state fragments with unrelaxed MOs.

The definition of the polarized state, on the other hand, takes advantage of the ALMO-CIS scheme we have previously developed.[66] In ALMO-CIS, the intrafragment relaxation of MOs due to the presence of other fragments is accounted for at the ground state level (via the SCF-MI approach), while the corresponding excited state of the supersystem, constructed as a superposition of intrafragment excitations, is computed based upon these absolutely localized orbitals. This polarized excited state relaxes the amplitudes on the excited fragment and also permits the excitation to spread to other fragments (though without charge transfer). Finally, the fully relaxed state is given by a standard CIS calculation for the entire system. The differences between the excitation energies evaluated at these intermediate levels (including the initial and the final) define the frozen, polarization, and charge transfer contributions to the shift in excitation energy of this specific fragment due to its interaction with the other molecules in the environment.

This method, to our knowledge, is the first EDA scheme designed for fully *ab initio* intermolecular interactions that involve a molecular complex in an excited state. It is most suitable for scenarios where the complex excitation is reasonably well-localized to a single fragment. In such cases, it reports on the modulation of molecular excited states by the surrounding environment. Illustrated by the proof-of-concept applications, useful insights on changes in excitation energies induced by intermolecular interactions are obtained by using this EDA method. For example, from the study of the $NeHe_N$ clusters, we find that the Pauli interaction between the excited neon and the ground state helium atoms is responsible for the blue shift in neon's $2p \rightarrow 3s$ excitation (when the Ne–He distances are greater than 2 Å), and for a hydrogen-bonding system such as the formamide-water complex, the diminished permanent electrostatics associated with the $n \rightarrow \pi^*$ transition turns out to be the primary reason for the blue shift in the corresponding excitation energy.

As a first effort to extend EDA schemes to intermolecular interactions involving molecules in their excited states, our method still has several limitations. (i) Total energies of excited states are not fully variational (MOs optimized in the ground state are employed for excited states). Therefore, the negative semi-definite terms in the ground state ALMO-EDA (polarization and CT) are indefinite for the exciplex (see Sec. II). Although this rarely occurs in practice, a scheme which ensures that these terms are negative semi-definiteness would be preferable. (ii) Our method is most appropriate for exciplexes where most excitation amplitude belongs to one fragment and connects to an excited state of that fragment in isolation. However, sometimes the fragment excited state does not exist in isolation [e.g., CTTS excitation of $Cl^-(H_2O)_N$]. In

other cases, the excited state may strongly couple with excitations in the environment that are close in energy (e.g., the exciton splitting effect mentioned in Sec. III B). (iii) The present EDA method can only handle one single excited fragment at separation, so cases involving multiple excited fragments would be an interesting future extension.

SUPPLEMENTARY MATERIAL

See supplementary material for the EDA results using CIS for the pyridine/pyrimidine-water complex systems.

ACKNOWLEDGMENTS

This work was supported by the Director, Office of Science, Office of Basic Energy Sciences, of the U.S. Department of Energy under Contract No. DE-AC02-05CH11231.

[1] J. Tomasi, B. Mennucci, and R. Cammi, Chem. Rev. **105**, 2999 (2005).
[2] M. M. Karelson and M. C. Zerner, J. Phys. Chem. **96**, 6949 (1992).
[3] J. Li, C. J. Cramer, and D. G. Truhlar, Int. J. Quantum Chem. **77**, 264 (2000).
[4] U. C. Singh and P. A. Kollman, J. Comput. Chem. **7**, 718 (1986).
[5] M. J. Field, P. A. Bash, and M. Karplus, J. Comput. Chem. **11**, 700 (1990).
[6] H. M. Senn and W. Thiel, Angew. Chem., Int. Ed. **48**, 1198 (2009).
[7] G. Fradelos and T. A. Wesołowski, J. Phys. Chem. A **115**, 10018 (2011).
[8] J. M. H. Olsen, C. Steinmann, K. Ruud, and J. Kongsted, J. Phys. Chem. A **119**, 5344 (2015).
[9] L. J. Nåbo, J. M. H. Olsen, N. Holmgaard List, L. M. Solanko, D. Wüstner, and J. Kongsted, J. Chem. Phys. **145**, 104102 (2016).
[10] M. J. Blandamer and M. F. Fox, Chem. Rev. **70**, 59 (1970).
[11] J. Jortner, M. Ottolenghi, and G. Stein, J. Phys. Chem. **68**, 247 (1964).
[12] J. A. Kloepfer, V. H. Vilchiz, V. A. Lenchenkov, and S. E. Bradforth, Chem. Phys. Lett. **298**, 120 (1998).
[13] L. Lehr, M. Zanni, C. Frischkorn, R. Weinkauf, and D. Neumark, Science **284**, 635 (1999).
[14] W. S. Sheu and P. J. Rossky, J. Am. Chem. Soc. **115**, 7729 (1993).
[15] D. Serxner, C. E. Dessent, and M. A. Johnson, J. Chem. Phys. **105**, 7231 (1996).
[16] H.-Y. Chen and W.-S. Sheu, J. Am. Chem. Soc. **122**, 7534 (2000).
[17] J. Kim, H. M. Lee, S. B. Suh, D. Majumdar, and K. S. Kim, J. Chem. Phys. **113**, 5259 (2000).
[18] J. Baik, J. Kim, D. Majumdar, and K. S. Kim, J. Chem. Phys. **110**, 9116 (1999).
[19] D. Majumdar, J. Kim, and K. S. Kim, J. Chem. Phys. **112**, 101 (2000).
[20] A. Stone, *The Theory of Intermolecular Forces* (OUP Oxford, 2013).
[21] P. Arora, L. V. Slipchenko, S. P. Webb, A. DeFusco, and M. S. Gordon, J. Phys. Chem. A **114**, 6742 (2010).
[22] L. V. Slipchenko, J. Phys. Chem. A **114**, 8824 (2010).
[23] D. Kosenkov and L. V. Slipchenko, J. Phys. Chem. A **115**, 392 (2010).
[24] T. A. Wesolowski and A. Warshel, J. Phys. Chem. **97**, 8050 (1993).
[25] T. A. Wesolowski, S. Shedge, and X. Zhou, Chem. Rev. **115**, 5891 (2015).
[26] J. Neugebauer, M. J. Louwerse, E. J. Baerends, and T. A. Wesolowski, J. Chem. Phys. **122**, 094115 (2005).
[27] P. Reinholdt, J. Kongsted, and J. M. H. Olsen, J. Phys. Chem. Lett. **8**, 5949 (2017).
[28] H. Nakata, D. G. Fedorov, S. Yokojima, K. Kitaura, M. Sakurai, and S. Nakamura, J. Chem. Phys. **140**, 144101 (2014).
[29] A. Davydov, *Theory of Molecular Excitons* (Springer, 2013).
[30] J. Frenkel, Phys. Rev. **37**, 17 (1931).
[31] J. M. Herbert, X. Zhang, A. F. Morrison, and J. Liu, Acc. Chem. Res. **49**, 931 (2016).
[32] S. Rybak, B. Jeziorski, and K. Szalewicz, J. Chem. Phys. **95**, 6576 (1991).
[33] B. Jeziorski, R. Moszynski, and K. Szalewicz, Chem. Rev. **94**, 1887 (1994).
[34] P. S. Żuchowski, R. Podeszwa, R. Moszyński, B. Jeziorski, and K. Szalewicz, J. Chem. Phys. **129**, 084101 (2008).
[35] K. Szalewicz, Wiley Interdiscip. Rev.: Comput. Mol. Sci. **2**, 254 (2012).
[36] E. G. Hohenstein and C. D. Sherrill, Wiley Interdiscip. Rev.: Comput. Mol. Sci. **2**, 304 (2012).
[37] K. Kitaura and K. Morokuma, Int. J. Quantum Chem. **10**, 325 (1976).
[38] K. Morokuma, Acc. Chem. Res. **10**, 294 (1977).
[39] T. Ziegler and A. Rauk, Theor. Chem. Acc. **46**, 1 (1977).
[40] T. Ziegler and A. Rauk, Inorg. Chem. **18**, 1558 (1979).
[41] M. von Hopffgarten and G. Frenking, Wiley Interdiscip. Rev.: Comput. Mol. Sci. **2**, 43 (2012).
[42] P. S. Bagus, K. Hermann, and C. W. Bauschlicher, Jr., J. Chem. Phys. **80**, 4378 (1984).
[43] W. J. Stevens and W. H. Fink, Chem. Phys. Lett. **139**, 15 (1987).
[44] P. Su and H. Li, J. Chem. Phys. **131**, 014102 (2009).
[45] P. Su, Z. Jiang, Z. Chen, and W. Wu, J. Phys. Chem. A **118**, 2531 (2014).
[46] Y. Mo, J. Gao, and S. D. Peyerimhoff, J. Chem. Phys. **112**, 5530 (2000).
[47] Y. Mo, L. Song, and Y. Lin, J. Phys. Chem. A **111**, 8291 (2007).
[48] Y. Mo, P. Bao, and J. Gao, Phys. Chem. Chem. Phys. **13**, 6760 (2011).
[49] Q. Wu, P. W. Ayers, and Y. Zhang, J. Chem. Phys. **131**, 164112 (2009).
[50] Q. Wu, J. Chem. Phys. **140**, 244109 (2014).
[51] R. Z. Khaliullin, E. A. Cobar, R. C. Lochan, A. T. Bell, and M. Head-Gordon, J. Phys. Chem. A **111**, 8753 (2007).
[52] P. R. Horn, E. J. Sundstrom, T. A. Baker, and M. Head-Gordon, J. Chem. Phys. **138**, 134119 (2013).
[53] P. R. Horn, Y. Mao, and M. Head-Gordon, Phys. Chem. Chem. Phys. **18**, 23067 (2016).
[54] A. J. Misquitta, R. Podeszwa, B. Jeziorski, and K. Szalewicz, J. Chem. Phys. **123**, 214103 (2005).
[55] G. Jansen, Wiley Interdiscip. Rev.: Comput. Mol. Sci. **4**, 127 (2014).
[56] A. J. Stone and A. J. Misquitta, Chem. Phys. Lett. **473**, 201 (2009).
[57] A. J. Misquitta, J. Chem. Theory Comput. **9**, 5313 (2013).
[58] K. U. Lao and J. M. Herbert, J. Chem. Theory Comput. **12**, 2569 (2016).
[59] S. N. Steinmann, C. Corminboeuf, W. Wu, and Y. Mo, J. Phys. Chem. A **115**, 5467 (2011).
[60] H. Stoll, G. Wagenblast, and H. Preubeta, Theor. Chem. Acc. **57**, 169 (1980).
[61] E. Gianinetti, I. Vandoni, A. Famulari, and M. Raimondi, Adv. Quantum Chem. **31**, 251 (1998).
[62] R. Z. Khaliullin, M. Head-Gordon, and A. T. Bell, J. Chem. Phys. **124**, 204105 (2006).
[63] P. R. Horn and M. Head-Gordon, J. Chem. Phys. **143**, 114111 (2015).
[64] P. R. Horn, Y. Mao, and M. Head-Gordon, J. Chem. Phys. **144**, 114107 (2016).
[65] Y. Mao, P. R. Horn, and M. Head-Gordon, Phys. Chem. Chem. Phys. **19**, 5944 (2017).
[66] K. D. Closser, Q. Ge, Y. Mao, Y. Shao, and M. Head-Gordon, J. Chem. Theory Comput. **11**, 5791 (2015).
[67] A. Dreuw and M. Head-Gordon, Chem. Rev. **105**, 4009 (2005).
[68] J. B. Foresman, M. Head-Gordon, J. A. Pople, and M. J. Frisch, J. Phys. Chem. **96**, 135 (1992).
[69] Q. Ge, Y. Mao, A. F. White, E. Epifanovsky, K. D. Closser, and M. Head-Gordon, J. Chem. Phys. **146**, 044111 (2017).
[70] J. Thirman and M. Head-Gordon, J. Chem. Phys. **143**, 084124 (2015).
[71] J. Thirman and M. Head-Gordon, J. Phys. Chem. A **121**, 717 (2017).
[72] M. A. Marques and E. K. U. Gross, Annu. Rev. Phys. Chem. **55**, 427 (2004).
[73] S. Van Gisbergen, J. Snijders, and E. Baerends, Comput. Phys. Commun. **118**, 119 (1999).
[74] M. E. Casida, J. Mol. Struct.: THEOCHEM **914**, 3 (2009).
[75] S. Hirata and M. Head-Gordon, Chem. Phys. Lett. **314**, 291 (1999).
[76] M. Head-Gordon, P. E. Maslen, and C. A. White, J. Chem. Phys. **108**, 616 (1998).
[77] Y. Shao, Z. Gan, E. Epifanovsky, A. T. Gilbert, M. Wormit, J. Kussmann, A. W. Lange, A. Behn, J. Deng, X. Feng, D. Ghosh, M. Goldey, P. R. Horn, L. D. Jacobson, I. Kaliman, R. Z. Khaliullin, T. Kuś, A. Landau, J. Liu, E. I. Proynov, Y. M. Rhee, R. M. Richard, M. A. Rohrdanz, R. P. Steele, E. J. Sundstrom, H. L. Woodcock, P. M. Zimmerman, D. Zuev, B. Albrecht, E. Alguire, B. Austin, G. J. O. Beran, Y. A. Bernard, E. Berquist, K. Brandhorst, K. B. Bravaya, S. T. Brown, D. Casanova, C.-M. Chang, Y. Chen, S. H. Chien, K. D. Closser, D. L. Crittenden, M. Diedenhofen, R. A. DiStasio, H. Do, A. D. Dutoi, R. G. Edgar, S. Fatehi, L. Fusti-Molnar, A. Ghysels, A. Golubeva-Zadorozhnaya, J. Gomes, M. W. Hanson-Heine, P. H. Harbach, A. W. Hauser, E. G. Hohenstein, Z. C. Holden, T.-C. Jagau, H. Ji, B. Kaduk, K. Khistyaev, J. Kim, J. Kim, R. A. King, P. Klunzinger, D. Kosenkov, T. Kowalczyk, C. M. Krauter, K. U. Lao, A. Laurent, K. V. Lawler, S. V. Levchenko, C. Y. Lin, F. Liu, E. Livshits, R. C. Lochan, A. Luenser, P. Manohar, S. F. Manzer, S.-P. Mao, N. Mardirossian, A. V. Marenich, S. A. Maurer, N. J. Mayhall, E. Neuscamman, C. M. Oana, R. Olivares-Amaya, D. P. O'Neill, J. A. Parkhill, T. M. Perrine, R. Peverati,

A. Prociuk, D. R. Rehn, E. Rosta, N. J. Russ, S. M. Sharada, S. Sharma, D. W. Small, A. Sodt, T. Stein, D. Stück, Y.-C. Su, A. J. Thom, T. Tsuchimochi, V. Vanovschi, L. Vogt, O. Vydrov, T. Wang, M. A. Watson, J. Wenzel, A. White, C. F. Williams, J. Yang, S. Yeganeh, S. R. Yost, Z.-Q. You, I. Y. Zhang, X. Zhang, Y. Zhao, B. R. Brooks, G. K. Chan, D. M. Chipman, C. J. Cramer, W. A. Goddard, M. S. Gordon, W. J. Hehre, A. Klamt, H. F. Schaefer, M. W. Schmidt, C. D. Sherrill, D. G. Truhlar, A. Warshel, X. Xu, A. Aspuru-Guzik, R. Baer, A. T. Bell, N. A. Besley, J.-D. Chai, A. Dreuw, B. D. Dunietz, T. R. Furlani, S. R. Gwaltney, C.-P. Hsu, Y. Jung, J. Kong, D. S. Lambrecht, W. Liang, C. Ochsenfeld, V. A. Rassolov, L. V. Slipchenko, J. E. Subotnik, T. Van Voorhis, J. M. Herbert, A. I. Krylov, P. M. Gill, and M. Head-Gordon, Mol. Phys. **113**, 184 (2015).
[78]C. Møller and M. S. Plesset, Phys. Rev. **46**, 618 (1934).
[79]R. Krishnan, J. S. Binkley, R. Seeger, and J. A. Pople, J. Chem. Phys. **72**, 650 (1980).
[80]M. J. Frisch, J. A. Pople, and J. S. Binkley, J. Chem. Phys. **80**, 3265 (1984).
[81]T. H. Dunning, Jr., J. Chem. Phys. **90**, 1007 (1989).
[82]R. A. Kendall, T. H. Dunning, Jr., and R. J. Harrison, J. Chem. Phys. **96**, 6796 (1992).
[83]J. R. Reimers and Z.-L. Cai, Phys. Chem. Chem. Phys. **14**, 8791 (2012).
[84]J.-D. Chai and M. Head-Gordon, Phys. Chem. Chem. Phys. **10**, 6615 (2008).
[85]R. J. Buenker and S. D. Peyerimhoff, Chem. Phys. Lett. **29**, 253 (1974).
[86]K. D. Closser and M. Head-Gordon, J. Phys. Chem. A **114**, 8023 (2010).
[87]K. von Haeften, T. Laarmann, H. Wabnitz, T. Möller, and K. Fink, J. Phys. Chem. A **115**, 7316 (2011).
[88]K. von Haeften, T. Laarmann, H. Wabnitz, and T. Möller, Phys. Rev. Lett. **87**, 153403 (2001).
[89]M. Joppien, R. Karnbach, and T. Möller, Phys. Rev. Lett. **71**, 2654 (1993).
[90]J. Gingell, N. Mason, H. Zhao, I. Walker, and M. Siggel, Chem. Phys. **220**, 191 (1997).
[91]E. B. Nielsen and J. A. Schellman, J. Phys. Chem. **71**, 2297 (1967).
[92]H. Basch, M. Robin, and N. Kuebler, J. Chem. Phys. **49**, 5007 (1968).
[93]N. De Silva, S. Y. Willow, and M. S. Gordon, J. Phys. Chem. A **117**, 11847 (2013).
[94]P. R. Rablen, J. W. Lockman, and W. L. Jorgensen, J. Phys. Chem. A **102**, 3782 (1998).
[95]G. A. Jeffrey and W. Saenger, *Hydrogen Bonding in Biological Structures* (Springer Science & Business Media, 2012).
[96]E. Baker and R. Hubbard, Prog. Biophys. Mol. Biol. **44**, 97 (1984).